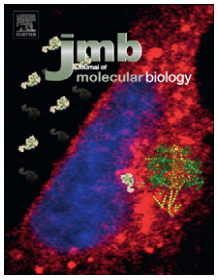

LRIG1 Extracellular Domain: Structure and Function Analysis

Yibin Xu [1,2], Priscilla Soo [2], Francesca Walker [1,3], Hui Hua Zhang [1], Nicholas Redpath [2,3], Chin Wee Tan [1,3], Nicos A. Nicola [2,3], Timothy E. Adams [4], Thomas P. Garrett [1,3], Jian-Guo Zhang [2,3] and Antony W. Burgess [1,3,5]

*1 - **Structural Biology Division,** The Walter and Eliza Hall Institute of Medical Research, Parkville, Victoria 3052, Australia*
*2 - **Cancer and Haematology Division,** The Walter and Eliza Hall Institute of Medical Research, Parkville, Victoria 3052, Australia*
*3 - **Department of Medical Biology,** University of Melbourne, Parkville, Victoria 3010, Australia*
*4 - **CSIRO Manufacturing Flagship,** Parkville, Victoria 3052, Australia*
*5 - **Department of Surgery,** RMH, University of Melbourne, Parkville, Victoria 3010, Australia*

***Correspondence to Jian-Guo Zhang and Antony W. Burgess:** The Walter and Eliza Hall Institute of Medical Research, 1G Royal Parade, Parkville, Victoria 3052, Australia. zhang@wehi.edu.au; tburgess@wehi.edu.au.*
http://dx.doi.org/10.1016/j.jmb.2015.03.001
Edited by T. Yeates

Abstract

We have expressed and purified three soluble fragments of the human LRIG1-ECD (*e*xtra*c*ellular *d*omain): the LRIG1-LRR (*l*eucine-*r*ich *r*epeat) domain, the LRIG1-3Ig (immunoglobulin-like) domain, and the LRIG1-LRR-1Ig fragment using baculovirus vectors in insect cells. The two LRIG1 domains crystallised so that we have been able to determine the three-dimensional structures at 2.3 Å resolution. We developed a three-dimensional structure for the LRIG1-ECD using homology modelling based on the LINGO-1 structure. The LRIG1-LRR domain and the LRIG1-LRR-1Ig fragment are monomers in solution, whereas the LRIG1-3Ig domain appears to be dimeric. We could not detect any binding of the LRIG1 domains or the LRIG1-LRR-1Ig fragment to the EGF receptor (EGFR), either in solution using biosensor analysis or when the EGFR was expressed on the cell surface. The FLAG-tagged LRIG1-LRR-1Ig fragment binds weakly to colon cancer cells regardless of the presence of EGFRs. Similarly, neither the soluble LRIG1-LRR nor the LRIG1-3Ig domains nor the full-length LRIG1 co-expressed in HEK293 cells inhibited ligand-stimulated activation of cell-surface EGFR.

Introduction

LRR (*l*eucine-*r*ich *r*epeat) proteins have been reported to modulate receptor activity in tissue stem cells [1–4]. LRIG1 was discovered in 1996 as an LRR/immunoglobulin (Ig) domain membrane glycoprotein that was upregulated when a mouse glial cell line was treated with retinoic acid [5]. LRIG1 appears to regulate the levels of ErbB family members [6] by increasing the degradation of these receptors [7]. Mutations to the intracellular domain of LRIG1 reduce its effects on EGFR degradation [7], and LRIG1 also increases the degradation of an oncogenic form of the EGFR(vIII), which is missing domain I and most of domain II [8]. Although it has been reported that cell-surface EGFR is necessary for the anti-proliferative action of the soluble ectodomain of LRIG1 [9], more recent reports indicate that the soluble form of LRIG1 inhibits the proliferation of glioma cells irrespective of the levels of the EGFR [10].

In the last decade, LRIG1 has been reported to interact with many receptor tyrosine kinases, GDNF/c-Ret [11], E-cadherin [12], JAK/STAT [13], c-Met [14,15], and the EGFR family [7,9] signalling systems. In some cases, LRIG1 is reported to reduce receptor levels by increasing the rates of degradation [7]; in other reports, LRIG1 appears to bind directly to the receptor kinase (e.g., the EGFR) [9]. These results

suggest that part of the action of LRIG1 on the EGFR family may be indirect [16]. At present, the broad specificity of action of LRIG1 and the reported opposing activity of LRIG3 [17] are difficult to understand.

The ectodomain of LRIG1 has two distinct regions, the proposed 15 LRRs (residues 41–494) and three Ig-like domains closer to the membrane (residues 494–781) [18]. We have produced three fragments of the ECD (*extra*cellular *d*omain) of human LRIG1: LRIG1-LRR, LRIG1-3Ig, and LRIG1-LRR-1Ig. Two of these LRIG1 fragments crystallised so that we were able to determine the detailed molecular structures. Using homology modelling based on the LINGO-1 structure [19], we have developed a structure for the entire LRIG1-ECD.

We have attempted to measure the interaction between the FLAG-tagged LRIG1-LRR-1Ig with membrane-associated human EGFR on A431 cells and SW480 colorectal cancer cells, but we could not detect any binding. Indeed, FLAG-tagged LRIG1-LRR-1Ig appeared to bind more strongly to SW620 colorectal cancer cells that do not express the EGFR [20] than to SW480 colorectal cancer cells that do express the EGFR. High concentrations of LRIG1 ectodomain fragments and EGFR did not interact on a gel-filtration column or on a biosensor surface. When we expressed full-length FLAG-tagged LRIG1 on A431 cells, we could extract and immunoprecipitate both LRIG1 and the EGFR individually, but the reciprocal immune precipitations did not detect any interaction between the proteins.

Apart from some limited indirect data from LRIG1 knockout mice [2,3,21], most of the LRIG1:EGFR interaction data reported in the literature are derived from overexpression systems [7]. The profound effects of LRIG1 on the expression levels of so many tyrosine kinase receptors raise a doubt that there is a specific, direct interaction between the ECDs of the EGFR and LRIG1. It is important to determine whether a correctly folded LRIG1 ectodomain interacts directly with the EGFR-ECD and/or whether LRIG1 associates with the EGFR on the cell surface. Despite some interesting proposals on the roles of LRR proteins [2], in particular, the role of LRIG1 as a negative modulator of EGFR family activation [2,22], we suggest that the signalling, stem cell biology, and physiology attributed to LRIG family members in mammalian systems need to be re-evaluated.

Results

Crystal structure of LRIG1-LRR domain

In our initial experiments, we could not express the native LRIG1-LRR domain (41–494) [23] in our baculovirus system; however, by mutating four residues at the N-terminus of the human LRR domain to the equivalent hydrophilic residues present in the zebrafish LRIG1 homologue (UniProt E7EZ01), to produce the analogue Pro42Ser43Arg44Ser69L-RIG1-LRR, we obtained excellent expression in Hi5 insect cells (i.e., >3 mg/L). Although none of these residues are conserved in either LRIG2[†] or LRIG3[‡], the crystal structure of the Pro42Ser43Arg44Ser69-L-RIG1-LRR domain (coding sequences 41–494) could be solved by molecular replacement using the atomic coordinates of decorin [24] as a search model. The coordinates were refined against data to 2.3 Å resolution. Data collection and structure refinement statistics for the LRIG1-LRR (residues 41–494) are summarised in Table 1.

The structure of LRIG1-LRR is crescent shaped, characteristic of other LRR protein structures (Fig. 1a). It contains 19 β-strands with 16 LRRs (numbered 1–16). There are 15 complete LRRs [1–15], each with 23–27 residues, where 11 LRRs have the 24-residue repeat [LxxLxLxxNxLxxLxxxx(Hϕ)xx(Hϕ)xx, where Hϕ is any hydrophobic amino acid residue]. LRR16 is only a partial repeat with a new pattern LxxLxIxSxxFx, where Ser appears to replace Asn in the consensus repeat (LxxLxLxxNxLxx). This Ser points towards the interior of the protein. It is interesting to note that although Asn residues are usually less conserved in LRR protein structures [25], these Asn are completely conserved in 15 of the 16 LRRs and adopt the same orientation in each repeat (Fig. 1a). The 16 LRR repeats are capped at both ends by cysteine-rich modules. The LRR-NT has two disulfide bridges (Cys41-Cys47 and Cys45-Cys54) that cross-link two anti-parallel β-strands (Fig. 1a). This N-capping motif (CxxxCxCxxxxxxC) at the start of the crescent is remarkably similar to that of decorin [24] and other extracellular LRR proteins [26]. The LRIG1-LRR-CT includes residues 444–490 with the pattern CxCx21Cx20C and resembles similar motifs in domain 2 of Slit2 [27], NgR [28], and the Netrin G ligands [29]. In addition to a common long α-helix (Cys446-Arg458) and the 310-helix at the C-terminus (Pro484-Ser486), LRIG1 has an additional β-strand (Val464-Thr467) that hydrogen bonds to the LRR16 repeat (Fig. 1a).

The five predicted N-glycosylation sites for the crystallised LRIG1-LRR (Asn74, Asn150, Asn246, Asn292, and Asn318) are all modified (Fig. 1b). The N-glycan on Asn74 is located on the concave face of LRIG1-LRR and the N-glycan on Asn292 is positioned on the edge of the concave groove towards the middle of the LRR. The presence of glycans on the concave face of the LRIG1-LRR also occurs in LINGO-1 [19] and would be expected to interfere with ligand binding to the N-terminal region of LRIG1. The other three glycosylated sites (Asn150, Asn246, and Asn318) are all located on one flank next to the concave face of LRIG1, leaving

Table 1. LRIG1-LRR and LRIG1-3Ig X-ray diffraction data collection and refinement statistics.

	LRIG1-LRR	LRIG1-3Ig
Data collection and processing		
Resolution (Å)	50–2.3 (2.39–2.3)	50–2.76 (2.91–2.76)
Wavelength (Å)	0.954	0.954
Space group	$P2_1\ 2_12_1$	$P4_3\ 2_12$
Unit cell dimensions (Å)		
a	38.94	121.04
b	94.76	121.04
c	169.43	115.8
Unique reflections	28,430 (3003)	22,552 (3112)
Redundancy	7.1 (7.4)	9.4 (9.3)
Completeness (%)	99.8 (99.9)	98.3 (89.2)
CC(1/2) (%) [25]	99.7 (57.5)	99.8 (29.5)
R_{merge}	13.3 (224.2)	16.7 (300)
Average $I/\sigma(I)$	9.21 (0.87)	11.68 (0.88)
Refinement		
Reflections for refinement/test	26,998/1387 (2.38–2.3)	21,374/1153 (2.88–2.76)
R/R_{free} (%)	20/25.48 (37.2/42.1)	20.47/25.33 (39.49/46.91)
rmsd angle (°)	0.76	0.870
rmsd bond (Å)	0.004	0.006
Mean *B*-factor (Å)	69.7	94.9
Non-hydrogen protein atom	3527	2232
Sugar atom	84	14
Water molecules	34	18
Ramachandran plot (%)		
Favoured region	94	95.1
Allowed region	5.8	4.9
Outlier region	0.2	0.0

Structural values in parentheses are for the last-resolution shell.

the other flank and convex surface of LRIG1-LRR sugar free.

Crystal structure of the LRIG1-3Ig domain

The LRIG1-3Ig domain expressed well in the Hi5 baculovirus/insect cell system. Crystals were obtained in space group $P4_32_12$, with one molecule in the asymmetric unit and a high solvent content (78%). The structure was determined by molecular replacement (see Materials and Methods) and refined to 2.76 Å resolution. The data collection and structure refinement statistics are summarised in Table 1. The crystal structure reveals that all three Ig domains belong to the I-type of the immunoglobulin superfamily (IgSF) [30], with the two anti-parallel β-sheets showing ABED and A′GFCC′ topology (Fig. 2).

LRIG1-3Ig is a rod-shaped molecule with Ig1 curving away by about 30° from the linear arrangement for alignment of the Ig2-Ig3 domains (Fig. 2a). The interdomain buried surface areas for the Ig domains are 421 $Å^2$ for Ig1-Ig2 and 432 $Å^2$ for Ig2-Ig3. The interface between Ig1 and Ig2 includes the side chains of Asn596 and Phe569 of Ig1 and Val597, His625, and Ser677 of Ig2 (Fig. 2b). The side chains form a network of five hydrogen bonds across the Ig1-Ig2 contact region. The detailed interactions of the Ig2-Ig3 contact region also include four hydrogen bonds, including the backbone carbonyl oxygen of Val689 and the ND2 atom of Asn719 in Ig3. The side chain of Leu690 in Ig2 makes close contact with the side chain of Leu769 in Ig3 (Fig. 2c).

Although there is only one molecule in the asymmetric unit, the LRIG1-3Ig fragment forms a dimer in the crystal through a crystallographic 2-fold axis. This dimer is consistent with gel-filtration chromatography measurements on the soluble protein (data not shown). The dimer interface is composed of two identical sites between the LRIG1-Ig1 and LRIG1-Ig2 domains and is predominantly hydrophobic in nature (Fig. 2d). The total surface area buried is 2691 $Å^2$ with a shape complementarity value of 0.63, which is typical for protein–protein interfaces for immunoglobulin dimers [31]. At this interface, the side chains of Val546, Val548, Met556, and Tyr558 in LRIG1-Ig1 insert into the pocket formed by residues Trp632, Phe640, Met648, Val650, and Phe657 in LRIG1-Ig2 (Fig. 2e). The phenyl ring of Phe545 in Ig1 makes close contact with residues Ala631, Asn633, and Thr673 from LRIG1-Ig2. In addition, the backbone N and O atoms of Trp632 form hydrogen bonds with the LRIG1-Ig1 backbone at Val546. In the crystal, these hydrogen bonds prevent Trp632 forming a further hydrogen bond with Asp639, accounting for the missing C′ strand in LRIG-Ig2.

The crystal structure reveals that all three Ig domains belong to the I-type of the immunoglobulin superfamily (IgSF) [30], with the two anti-parallel β-sheets showing ABED and A′GFCC′ topology (Fig. 3). The LRIG1-Ig1 (D1, residues 494–596) has extended strands βD and βE, whereas Ig2 (D2, residues 597–690) has a missing strand βC′. The Ig1 domain of LRIG1 closely resembles the Ig1 domain of Axl [26] (PDB entry 2C5D) with an rmsd of 1.6 Å for 92 C^α atoms and yet there is only 16% amino sequence identity. In the crystal structure of the Axl-Gas6 complex [32], the extended strand βD of Axl-Ig interacts with the strand βB of the vitamin-K-dependent protein Gas6. Structural superpositions (Fig. 3) suggest that Ig2 and Ig3 of LRIG1 are more similar to each other (rmsd = 1.3 Å for 87 C^α atoms, 31% amino acid sequence identity) than to Ig1 (Ig2 > Ig1, rmsd = 1.4 Å for 80 C^α atoms; Ig3 > Ig1, rmsd = 1.5 Å for 82 C^α atoms).

Effect of LRIG1 on the activity of the EGFR

We investigated the interaction (both functionally and physically) between LRIG1 and the EGFR and whether the soluble fragment LRIG1-LRR or LRIG1-3Ig from the ECD inhibited phosphorylation or signalling in a cell line that overexpresses the EGFR and constitutively stimulates phosphorylation of Erk1/2 (MAPK1/2). A431 cells express $>10^6$ EGFR per cell [33]; thus, it is easy to detect auto-tyrosine-

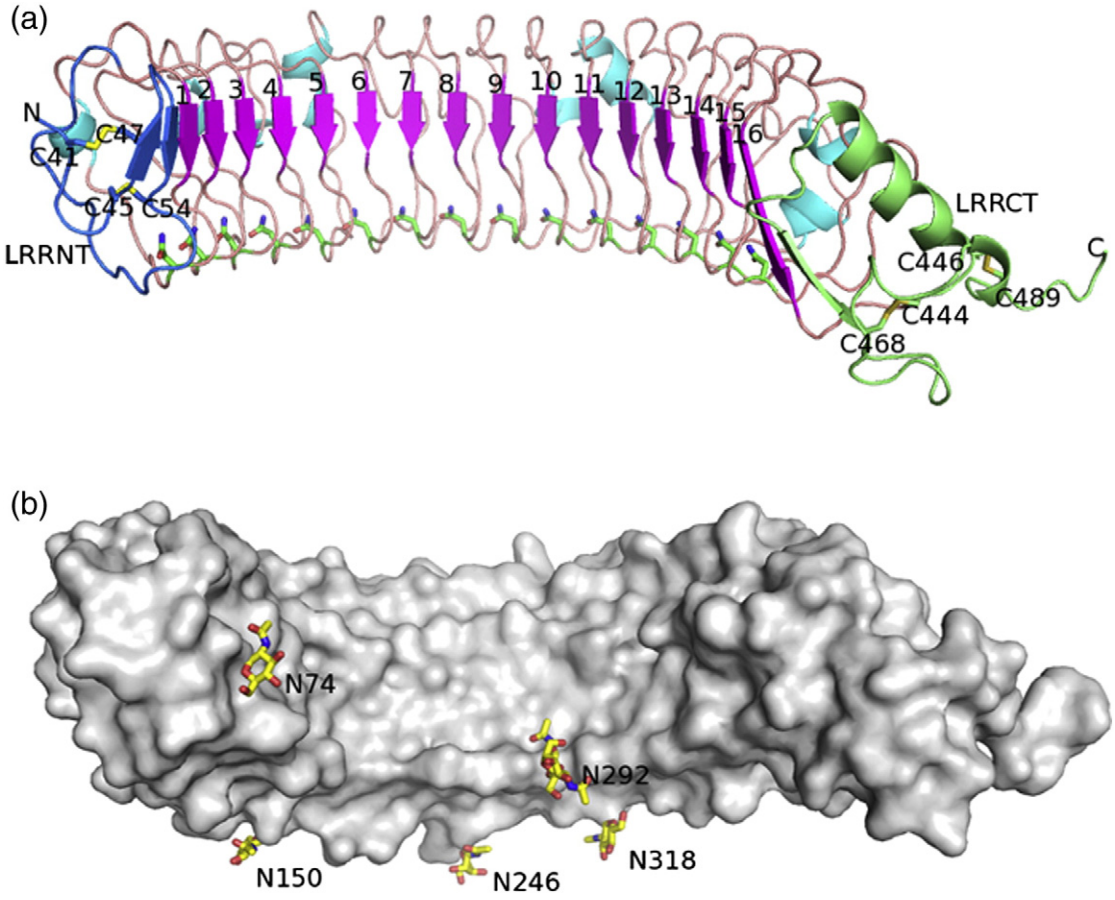

Fig. 1. Crystal structure of LRIG1-LRR domain. (a) Ribbon diagram of LRR. LRR-NT and LRR-CT are coloured marine and lime, respectively. The β-strands are coloured magenta; helixes are coloured cyan and loops are coloured salmon. The disulfide bonds in both LRR-NT and LRR-CT and the 15 Asn residues in each LRR repeat are shown in wireframe representation; (b) five NAG glycosylation sites on LRR surface are shown in wireframe representation: oxygen, red; nitrogen, blue; and carbon, yellow.

phosphorylation of the EGFR. Neither the LRIG1-LRR nor the LRIG1-3Ig ECD fragments inhibited the autophosphorylation of the EGFR nor the phosphorylation of Erk1/2 (Fig. 4). To test whether full-length, membrane-associated LRIG1 might be required to observe an effect on the EGFR, we transfected the A431 cells with FLAG-tagged, full-length, native LRIG1 and cultured the cells for 48 h. Interaction between LRIG1 and EGFR was measured by immunoprecipitation using anti-FLAG M2 beads (Fig. 5). As expected, the FLAG-tagged LRIG1 was detected on the Western blot analysis of the anti-FLAG M2 immunoprecipitates, but there was only a small amount of associated EGFR (as detected by Mab806 [34]; Fig. 5). The presence of FLAG-LRIG1 did not alter either the level of EGFR or the level of tyrosine phosphorylation of the EGFR on A431 cells (Fig. 5). In case that the high level of EGFR on A431 cells was interfering with our ability to detect an interaction between the EGFR and LRIG1, we repeated the experiments in HEK293 cells transfected with FLAG-Myc-tagged LRIG1 and/or the full-length EGFR (Fig. 6). The anti-Myc immunoprecipitation from LRIG1 transfected cells contained detectable LRIG1 (detected on the Western with the anti-FLAG antibody). The cells transfected with FLAG-tagged EGFR also expressed detectable levels of EGFR running slightly slower than LRIG1 (Fig. 6); however, there was no detectable FLAG-EGFR in the LRIG1 immunoprecipitates from the FLAG-Myc-tagged LRIG1:FLAG-tagged EGFR double transfectants (Fig. 6).

Staining of colon cancer cells with FLAG-tagged LRIG1-LRR-1Ig

It has been reported that LRIG1 binds specifically to cells overexpressing the EGFR [9]. We have investigated using fluorescence microscopy the binding of FLAG-tagged LRIG1-LRR-1Ig to two colon cancer cell lines: one expressing the EGFR

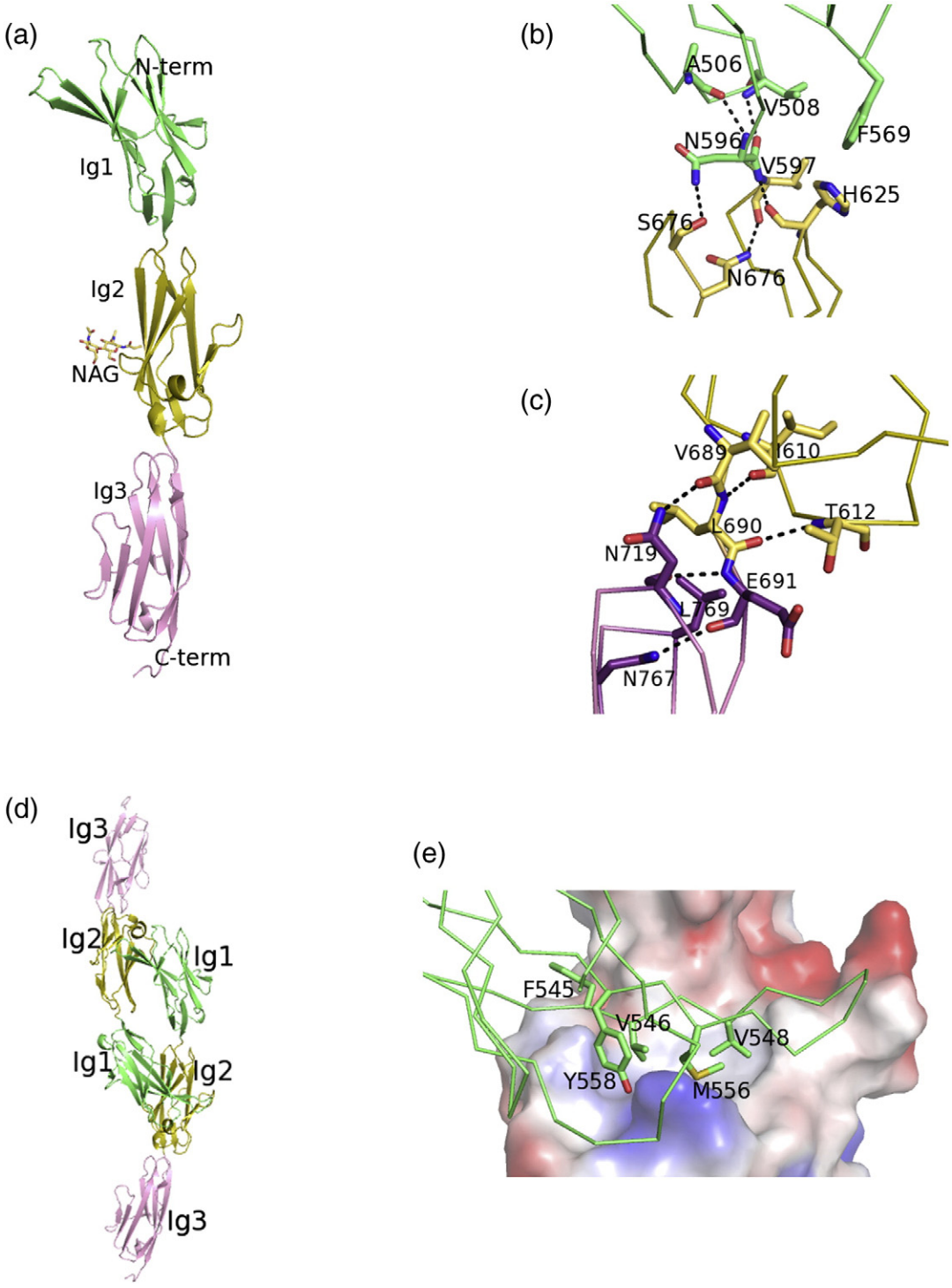

Fig. 2. Crystal structure of LRIG1-3Ig. (a) Ribbon diagram of LRIG1-3Ig. Ig1 is coloured lime; Ig2, olive; and Ig3, pink; the *N*-acetylglucosamine is shown as a wireframe representation and the atoms are coloured as follows: nitrogen, blue; oxygen, red; carbon, olive. (b and c) Residues involved in the interdomain regions of the Ig1-Ig2 interface and Ig2-Ig3 interface, respectively: oxygen, red; nitrogen, blue; carbon, lime (Ig1), olive (Ig2), and pink (Ig3); hydrogen bonds are depicted as black broken lines; (d) ribbon diagram of LRIG1-3Ig crystallographic dimer. Domains are coloured as in (a); (e) the Ig1-Ig2 dimer interface: residues Phe545, Val546, Val548, Met556, and Tyr558 of one Ig1 are displayed against the surface electrostatic potential of the Ig2 domain of the other chain: red is negatively charged and blue is positively charged.

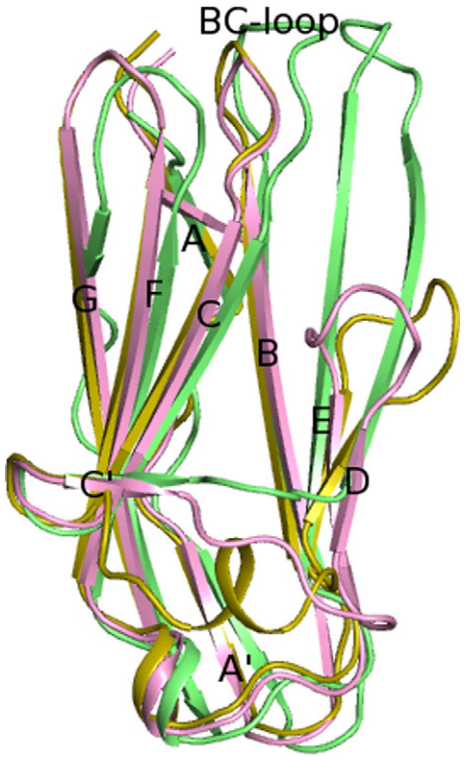

Fig. 3. Structural superposition of three individual Ig domains. Domains are depicted as ribbons with the strands labelled as follows: Ig1, lime; Ig2, olive; and Ig3, pink.

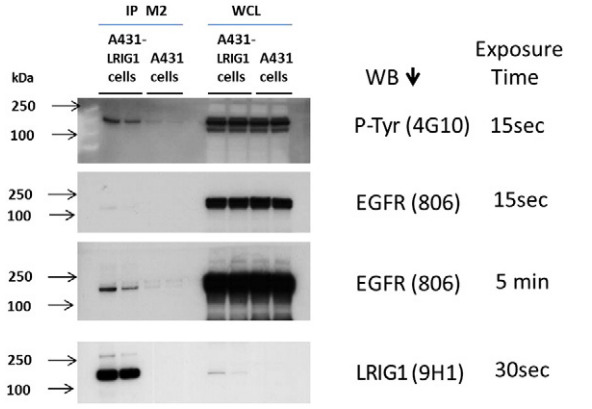

Fig. 5. Limited interaction between full-length LRIG1 and the EGFR on A431 cells. A431 cells were transfected with FLAG-tagged LRIG1. Whole cell lysates (WCL) were incubated with anti-FLAG M2-agarose beads. Bound proteins and WCL were separated by SDS-PAGE, followed by Western blot analysis using mouse anti-phosphotyrosine mAb 4G10 (top panel), mouse anti-EGFR mAb 806 (middle panel), and anti-FLAG mAb 9H1 (bottom panel). Lanes 1 and 3: FLAG peptide elution from LRIG1-M2 beads; lanes 2 and 4: SDS elution from LRIG1-M2 beads. lane 5: WCL of A431 cells transfected with LRIG1; lane 6: WCL of A431 cells transfected with LRIG1 after M2-agarose depletion; lane 7: WCL of A431 cells transfected with control plasmid; lane 8: WCL of A431 cells transfected with control plasmid after M2-agarose depletion.

(SW480 cells) [20] and the other one documented to lack the EGFR, SW620 cells [20,35]. As expected, in our immunofluorescence assay, anti-EGFR antibody detected EGFR on SW480 cells (Fig. 7a) but there was no staining associated with the SW620 cells (Fig. 7a). Treatment of the SW480 cells with EGF led to the downregulation (internalisation) of the EGFR (see Fig. 7a and b). This downregulation was same whether or not LRIG1-LRR-1Ig was present (Fig. 7a). Treatment of the SW480 cells with FLAG-tagged LRIG1-LRR-1Ig alone did not alter the level of EGFR detected on the SW480 cells (Fig. 7a). In contrast, the interaction of FLAG-tagged LRIG1-LRR-1Ig to SW480 cells or SW620 cells was not above background levels (Fig. 7b), indicating that any low level interaction of LRIG1 with the cell surface is independent of the level of expression of the EGFR. Similar staining patterns were also observed with the FLAG-tagged LRIG1-LRR domain (data not shown).

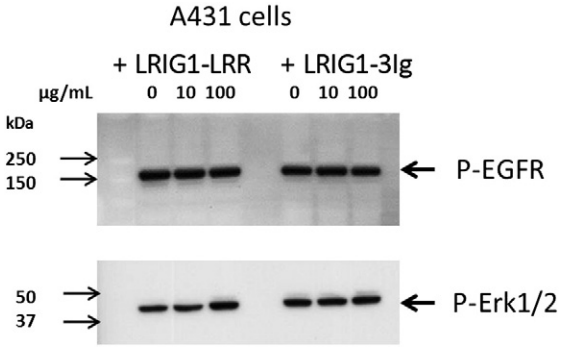

Fig. 4. No inhibition of EGFR signalling in A431 cells by LRIG1-LRR or LRIG1-3Ig. A431 cells were treated for 2 h at 37 °C with either recombinant LRIG1-LRR or LRIG1-3Ig at 0, 10, and 100 µg/mL, as indicated. Cells were lysed as described in Materials and Methods. Protein extracts were separated by SDS-PAGE, followed by Western blot analysis using anti-phosphotyrosine antibody 4G10 (top panel) and anti-Erk1/2 antibody (bottom panel).

Interaction between LRIG1-LRR and the EGFR ECD

Even when mixed at high concentration (>1 mg/mL for each protein), FLAG-tagged LRIG1-LRR and a high-affinity form of the EGFR-ECD (i.e., $EGFR_{1–501}$-Fc) did not appear to interact (Fig. 8). Gel-filtration analysis showed that, when the mixture was chromatographed on Superdex 200, both proteins eluted at their expected positions and that no LRIG1:EGFR complex could be detected at higher molecular weights (Fig. 8, inset).

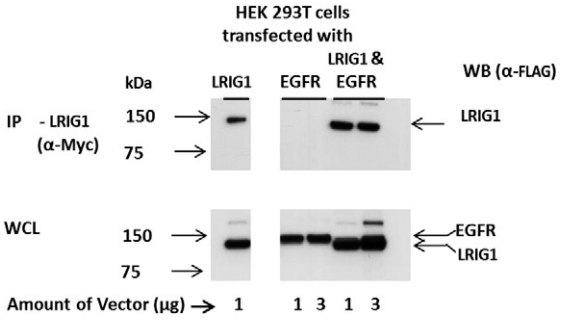

Fig. 6. No detectable interaction between full-length LRIG1 and EGFR on HEK293T cells. Top panel: Western blot analysis of LRIG1 immunoprecipitates (anti-Myc, mAb 9E10) from whole cell lysates (WCL) of HEK293T cells transfected with the following: lane 1, FLAG-Myc-tagged LRIG1; lane 2, FLAG-tagged EGFR (1 μg of cDNA); lane 3, FLAG-tagged EGFR (3 μg of cDNA); lane 4, FLAG-Myc-tagged LRIG1 and FLAG-tagged EGFR (1 μg of each cDNA); and lane 5, FLAG-Myc-tagged LRIG1 and FLAG-tagged EGFR (3 μg each cDNA). Blots were developed with the anti-FLAG mAb 9H1. Bottom panel: Western blot analysis of WCL from HEK293T cells transfected with the following: lane 1, FLAG-Myc-tagged LRIG1 (1 μg of cDNA); lane 2, FLAG-tagged EGFR (1 μg of cDNA); lane 3, FLAG-tagged EGFR (3 μg of cDNA); lane 4, FLAG-Myc-tagged LRIG1 and FLAG-tagged EGFR (with 1 μg of each cDNA); and lane 5, FLAG-Myc-tagged LRIG1 and FLAG-tagged EGFR (with 3 μg each cDNA). Blots were developed with the anti-FLAG mAb 9H1.

Similar experiments were repeated for the LRIG1-3Ig fragment (at 0.5 mg/mL) by mixing with the $EGFR_{1–501}$ or $EGFR_{1–621}$ ECD. Again, no LRIG1-3Ig:EGFR-ECD complex was detected by gel-filtration chromatography.

If the interactions between EGFR and LRIG1 are low affinity, gel filtration can allow dissociation of complexes. Consequently, we investigated the interaction of an LRIG1-LRR-1Ig-ECD fragment and EGF with two forms of immobilised EGFR-ECD. In these experiments, either $EGFR_{1–621}$ or $EGFR_{1–501}$ was coupled to the biosensor chip and different dilutions of either the LRIG1-LRR-1Ig-ECD fragment (0.25–8 μM) or EGF (3–200 nM) were injected into the fluid flowing over the chip (see Fig. 9). Both forms of the EGFR interacted with the EGF (Fig. 9c and d); as expected, $EGFR_{1–621}$ had a low binding affinity for EGF, whereas the $EGFR_{1–501}$-Fc bound EGF tightly [36]. In contrast, the LRIG1-LRR-1Ig-ECD fragment failed to interact with either $EGFR_{1–621}$ or $EGFR_{1–501}$ (see Fig. 9a and b). These experiments were repeated with the LRIG1-3Ig-ECD fragment (see Supplementary Fig. 3a–d); again, EGF bound to the receptor, but there was no detectable interaction with either of the EGFR-ECD fragments even at the highest concentration of this fragment (8 μM).

Discussion

The crystallisation of full-length, glycosylated ectodomains of cell-surface receptors can be problematic: often, there is variability in the glycosylation and even the orientation of the subdomains can be context dependent. LRRs fold into several canonical forms producing flat surfaces capable of participating in protein–protein interactions [25]. As is the case for LINGO-1 [19], both the concave and convex surfaces of the LRIG1-LRR domain are flat, but the concave surface is glycosylated, whereas the convex surface is free of glycosylation. Both structures have N-terminal caps and Ig-like domains at the C-terminus. When the LINGO-1-LRR and LRIG1 three-dimensional structures are aligned at the C-terminal region, the N-terminal region of LRIG1 diverges from the LINGO-1-LRR by 40 Å (see Supplementary Fig. 2). The prominent bulge at the C-terminus of the LINGO-1-LRR [19] is not as prominent in the LRIG1-LRR; however, the conformation of the region linking the LRR and Ig-like domains is similar in the two structures. The structural homology between the LINGO-1-Ig1 and the LRIG1-Ig1 domains suggests a model for the juxtaposition of the LRR domain and the Ig-like domains in LRIG1, where the LRR domain would be projected away from the cell surface (Supplementary Fig. 1). Analysis of LRIG1 species homology does not reveal any strongly conserved regions of the surface. The LRIG1-LRR:LRIG1-LRR fragment interactions in the crystal lattice occur between the terminal residues and do not appear to occlude sufficient surface area to indicate any physiological interaction sites.

Our attempts to detect an interaction between the LRIG1 and the EGFR were not successful. We tried measuring a direct interaction between LRIG1-ECD fragments and two soluble forms of the EGFR: $EGFR_{1–621}$-ECD or the $EGFR_{1–501}$ or the $EGFR_{1–501}$-Fc. All of the molecules were folded correctly, but no interaction was detected by gel filtration or biosensor analysis. The soluble LRIG1-ECD fragments bound weakly, if at all, to colon cancer cell lines and the level of these interactions was not influenced by the presence of EGFRs.

By transfecting full-length LRIG1 into HEK293 cells that were overexpressing members of the EGFR family (EGFR, ErbB2, ErbB3, and ErbB4), others have reported pull-down of LRIG1:EGFR, LRIG1:ErbB2, LRIG1:ErbB3, and LRIG1:ErbB4 complexes [7]; effects of LRIG1 on cell proliferation; and effects of LRIG1 on cell-surface EGFR levels, autophosphorylation, and signalling. Surprisingly, the EGFR pulled down full-length LRIG1, ΔLRR-LRIG1, and ΔIg-LRIG1 but not ΔLRR-ΔIg-LRIG1; that is, the EGFR appeared to interact significantly with both the LRR and 3Ig domains. The intracellular domain of LRIG1 did not interact with the EGFR [7]. However, LRIG1 can negatively

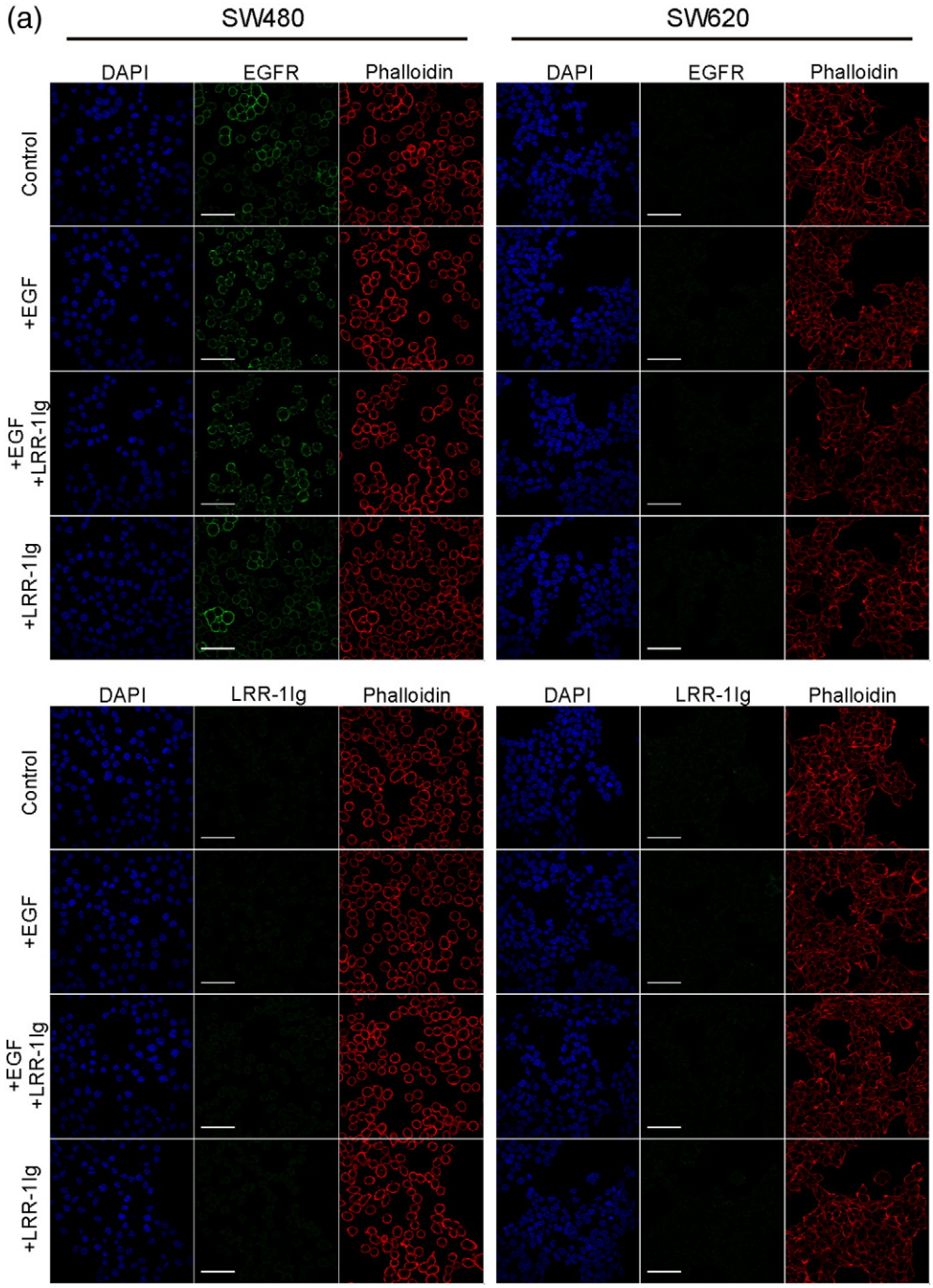

Fig. 7. Analysis of the interaction between FLAG-tagged LRIG1-LRR-1Ig with the SW480 ($EGFR^+$) and SW620 ($EGFR^-$) colon cancer cell lines. The cells were cultured in Ibidi chamber slides (5×10^3/well) for 3 days then stimulated with or without EGF (100 ng/mL) at 37 °C for 15 min. The cells were incubated with or without FLAG-LRIG1-LRR-1Ig (1 μM) at 4 °C for 45 min, and then with either the mouse antibody mAb528 (to detect the human EGFR) or the mouse anti-FLAG tag M2 antibody (to detect the FLAG-LRIG1-LRR-1Ig). (a) Antibody binding was detected with Alexa 488-labelled anti-mouse Ig and the cells were counterstained with 4′,6-diamidino-2-phenylindole and phalloidin. (b) The mean and relative fluorescence levels for the cells in three separate fields for each condition were quantitated as described previously [55]. The results from two independent experiments (red and blue bars) are presented. FLAG-tagged LRIG1-LRR-1Ig was abbreviated as LRR-1Ig.

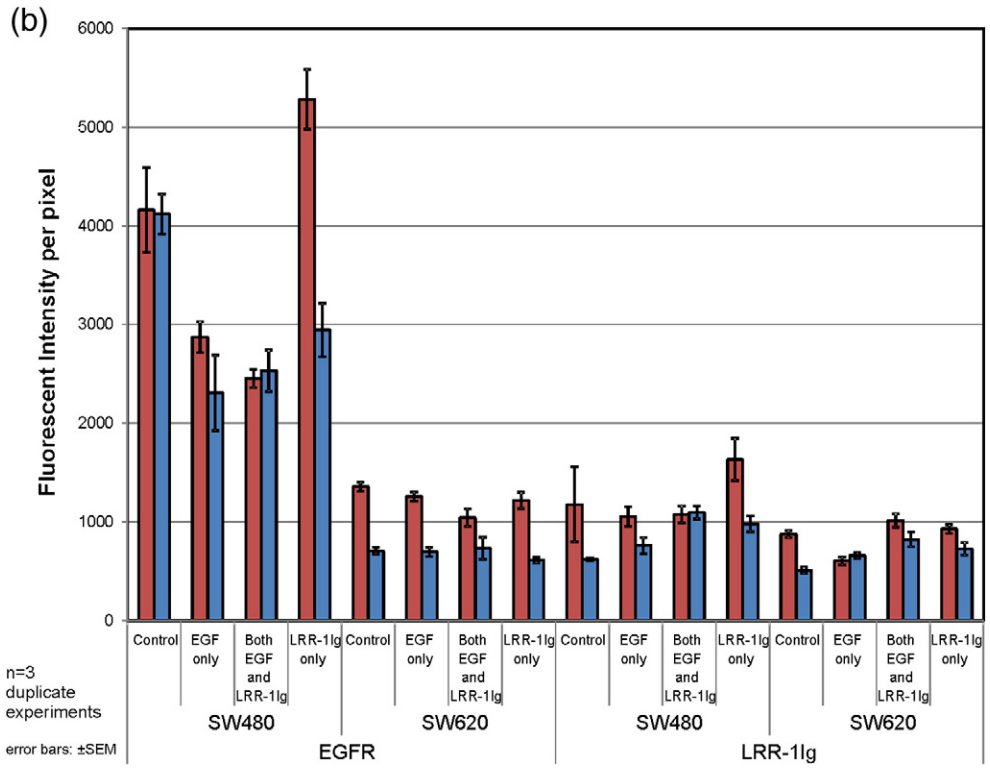

Fig. 7 (*continued*).

regulate the oncogenic Δ2-7EGFR [8], which lacks a significant portion of the EGFR ectodomain. Our attempts to obtain similar evidence for an LRIG1-EGFR interaction on the surface of A431 or HEK293 cells were unsuccessful. There were no significant levels of the EGFR in the LRIG1 pull-downs from A431 or HEK293 cells overexpressing both proteins nor could we detect an inhibitory effect of LRIG1 on ligand-induced EGFR signalling.

Reports on the actions of LRIG1 range from direct binding to the EGFR [9] to modulation of cell-surface levels by inducing degradation and by inhibiting

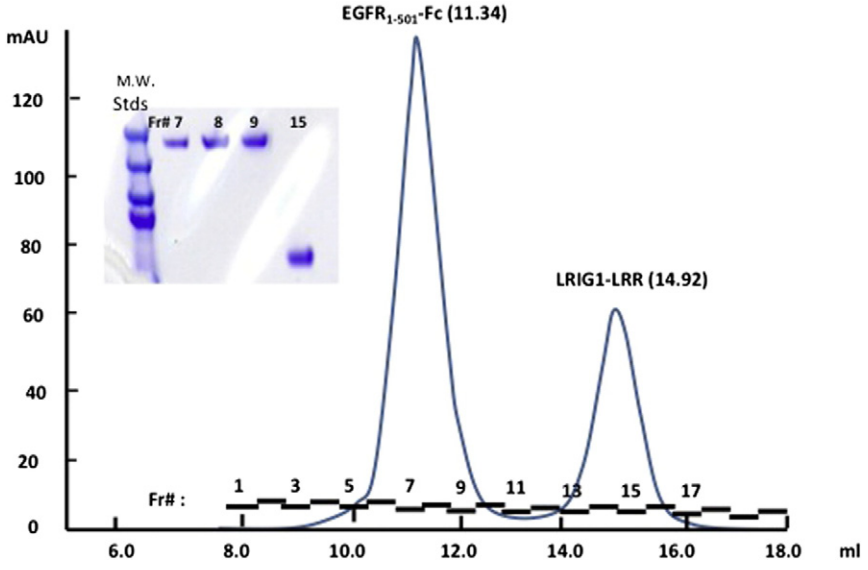

Fig. 8. Gel-filtration analysis of FLAG-tagged LRIG1-LRR and $EGFR_{1–501}$-Fc. A mixture of FLAG-tagged LRIG1-LRR and $EGFR_{1–501}$-Fc was loaded on to a Superdex 200 gel-filtration column and the fractions were analysed for both proteins. No complex was detected. *y*-Axis indicates absorbance unit (mAU) at 280 nm.

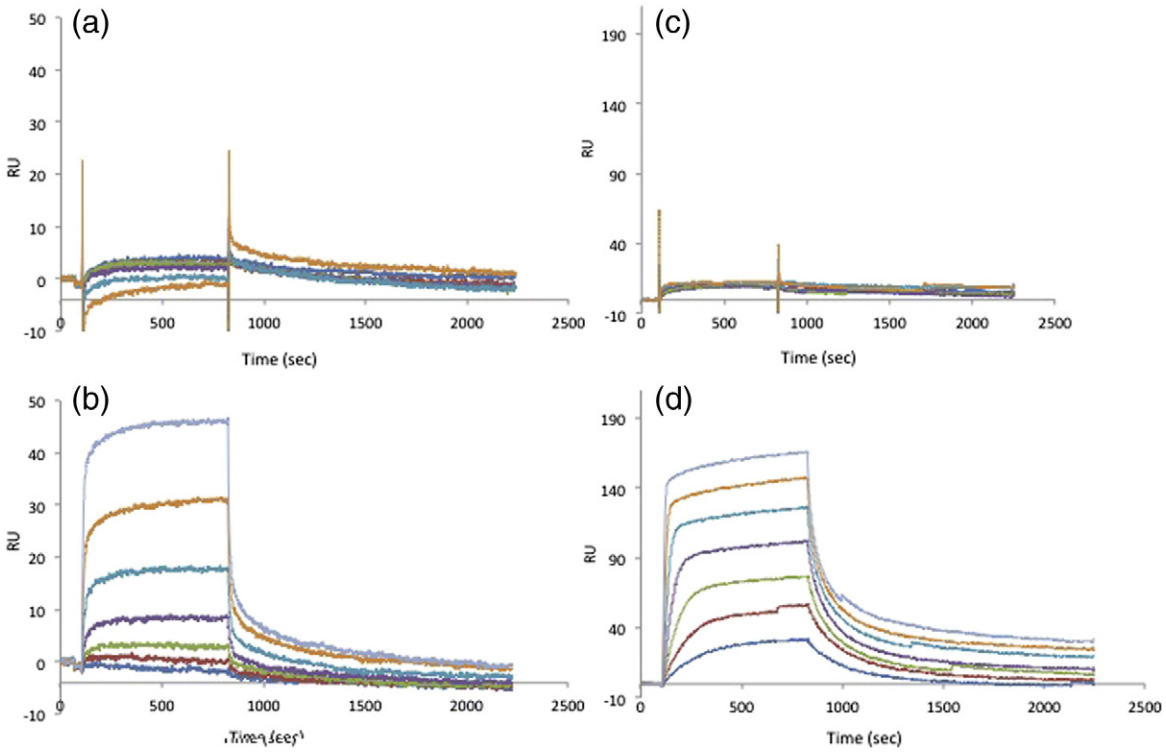

Fig. 9. Biosensor analysis of LRIG1-LRR-1Ig fragments and the EGFR-ECD. Various concentrations of LRIG1-LRR-1Ig fragment (from 8 μM to 0.25 μM in 2-fold dilutions) (a and c) and EGF (from 200 nM to 3.13 nM in 2-fold dilutions) (b and d) were injected over immobilised $EGFR_{1–621}$ (a and b) and $EGFR_{1–501}$ (c and d). The calculated K_D values for EGF binding to $EGFR_{1–621}$ and $EGFR_{1–501}$ were 140 nM and 8 nM, respectively. The results shown are representative of two experiments.

transcription and to direct interactions with ErbB2, ErbB3, c-Met [9], and c-Ret [12]. LRIG1 has been reported to promote cell–cell adhesion [12]. A significant physiological action has been proposed for LRIG1 in intestinal stem cells; that is, LRIG1 suppresses the activity of the EGFR [2,21]. In cancers, the decrease in LRIG1 levels has been proposed as a direct stimulus for cancer stem cell self-renewal and proliferation [6,9,21,37–39]. However, in other cancers, LRIG1 is overexpressed without any clear tumour suppressor effects [40].

Although the LRIG1 protein in our structure function studies was expressed in insect cells and thus may have a different glycosylation pattern, our failure to detect any direct or indirect interaction between LRIG1 and the EGFR expressed in human cells suggests that our results with LRIG1-LRR, LRIG1-LRR-1Ig, and LRIG1-3Ig in solution are not simply due to over glycosylation.

It is important to establish definitively the roles of LRIG1 in epithelial stem cells [2] and whether it has a direct role in tumour suppression. A recent paper has reported opposing effects of LRIG1 and LRIG3 on the turnover of the EGFR and ErbB2 [17]. Indeed, Rafidi's report suggests that LRIG1 can induce the degradation of LRIG3 and thus decrease the cell-surface levels of ErbB3 [17].

Since our structural results indicate that our LRIG1-ECD is correctly folded, we expected to detect the interaction with the EGFR on the cell surface. All of the previous studies used cell lines and systems where either the LRIG1 or the HER family members are overexpressed as recombinant proteins. It is important that physiological systems and reagents that will allow the analysis of the effects of LRIG1 expression, turnover, or modification in stem cell populations are developed. Initial reports on transgenic mice where LRIG1 has been knocked out indicate that the presence of LRIG1 leads to lower levels of the EGFR and EGFR-associated tyrosine phosphorylation [4]. In mice where LRIG1 has been knocked out, there are significant increases in the levels of EGFR family members in the basal crypt cells [4]; however, the changes in EGFR phosphorylation are less dramatic. Similarly, the effects on cell production within a crypt appear to be modest. In $LRIG1^{-/-}$ mice, the villus cell populations appear to be normal, but there seems to be increased cell numbers and turnover in the small intestinal crypts. The overall cellularity of colon crypts in mice appears to be less

perturbed when LRIG1 is knocked out. Interestingly, in some strains of mice, there is a 50% increase in the circumference of the intestines when LRIG1 is knocked out [4]; this increase in circumference corresponds closely to the increase in the width of the crypt base when LRIG1 is lost. However, in a similar experiment where LRIG1 is knocked out in mice with a different genetic background, no significant change in the size of the colon was detected [41]. It is interesting to note that although Wong *et al*. observed that the LRIG1$^{-/-}$ intestinal crypt morphology could return to normal when the mice were crossed on to a wa-2 background (i.e., the EGFR was kinase defective) [4], only a proportion of the crypts reverted.

The most convincing report on the influence of LRIG1-ECD on the activity of the EGFR family comes from data on HeLa cells, A431 cells, and MDA-468 cells [9]. Purified LRIG1-ECD or LRIG1-ECD secreted by HEK293 cells inhibited the proliferation of A431, HeLa, and MDA-468 cells (1.5- to 3-fold after 3–6 days in culture). A decorin-glycosylated fusion analogue of LRIG1-ECD was more potent than wild-type LRIG1-ECD, but both proteins appeared to inhibit cell proliferation. Furthermore, LRIG1-ECD inhibited the proliferation of CHO-K1 cells expressing the EGFR (by 50% after 2 days), but not wild-type CHO-K1 cells. The binding affinity of the LRIG1-ECD to A431 cells (~10 nM) correlated well with the IC_{50} for inhibition of Y1068 phosphorylation in the same cells; however, the inhibitory effect of the LRIG1-ECD on EGF-stimulated EGFR phosphorylation or Erk1/2 activation was less potent.

Despite producing and purifying appropriately folded LRIG-ECD fragments, our results are in contrast to the data reported by Goldoni *et al*. [9], as we could not detect direct binding of the LRIG1-LRR to the sEGFR-ECD or EGFR on the cell surface. Similarly, Johansson *et al*. observed an anti-proliferative effect of LRIG1, whether or not glioma cells expressed the EGFR [10]. Nor could we detect an effect of soluble, purified LRIG1-ECD, or co-expressed, full-length LRIG1 on the levels of EGFR, the phosphorylation of the EGFR kinase, or on the activation of EGFR signalling. Particularly worrying are our results and the results of others [10] indicating that the low level of binding of soluble LRIG1-LRR-1Ig to cells is not dependent of the cell-surface levels of the EGFR, suggesting that other cell-surface interactions may lead to interactions that interfere with our ability to conclude that LRIG1 is a physiological regulator of the EGFR family. Before we can conclude that LRIG1 is a functional or pan-ErbB inhibitor, the effects of LRIG1 on EGFR; ErbB2, ErbB3, and/or ErbB4 levels; phosphorylation; and signalling need to be measured by comparing epithelial stem cells with wild-type levels of LRIG1 with the same cells where LRIG1 has been deleted [42].

Materials and Methods

Expression and purification of proteins

Synthetic DNAs (GenScript) corresponding to human LRIG1-LRR (residues 41–494, AB050468) and LRIG1-3Ig (residues 494–781) were cloned into the modified vector [43]. Each construct contained a C-terminal TEV cleavage site [44] followed by the FLAG-tagged sequence [45]. To achieve high-level expression of LRIG1-LRR, we omitted the signal sequence and placed four residues (42–44 and 69) at the N-terminus; that is, C_{41}AAACTCAGDSLDCGG RGLAALPGDLPSW was replaced with C_{41}PSRCTCA GDSLDCGGRGLAALPGDLPSS. These fragments of the LRIG1-LRR and LRIG1-3Ig ectodomains were expressed in Hi5 insect cells and purified by anti-FLAG M2 beads (Sigma-Aldrich). The proteins were further purified by gel filtration in 20 mM Tris–HCl (pH 8.5) and 100 mM NaCl.

The cloning, expression, and purification of FLAG-tagged LRIG1-LRR-1Ig, FLAG-tagged $EGFR_{1–501}$ and FLAG-tagged $EGFR_{1–621}$ were similar to that of the LRIG1-LRR and LRIG1-3Ig fragments as described above. Briefly, synthetic DNAs (Genescript) corresponding to human LRIG1-LRR-1Ig (residues 41–596), $EGFR_{1–501}$ (residues 1–501), and $EGFR_{1–621}$ (residues 1–621) were cloned into the modified vector and expressed in Hi5 insect cells and purified by anti-FLAG M2 beads (Sigma-Aldrich). The proteins were further purified by gel-filtration chromatography on a pre-packed Superdex 200 column (GE Healthcare) in 20 mM Hepes (pH 7.4), 150 mM NaCl, and 3 mM EDTA (*e*thylene*d*iamine*t*etraacetic *a*cid).

Crystallisation and data collection

A crystallisation screen was performed at the Collaborative Crystallisation Centre, CSIRO, Parkville. Although high-quality crystals for LRIG1-LRR were grown at 18% PEG (*poly*e*t*hylene *g*lycol) 4000 and 0.1 M Hepes (pH 7.5), the best crystals of LRIG1-LRR, which diffracted to 2.3 Å, were grown at 16% PEG 4000 and 0.1 M Hepes (pH 7.0) with 10 mM Taurine by streaked seeding from the initial conditions. LRIG1-3Ig crystals were grown from 0.8 M sodium succinate (pH 7.0) at 5 mg/mL. All X-ray diffraction data were collected on the Australian Synchrotron microcrystal beamline MX2 [46]. The resultant data sets were processed and scaled with the XDS package [47]. The resolution cutoff was set on the basis of the Karplus CC(1/2) parameter [48]. The crystal statistics are summarised in Table 1.

Structure determination and refinement

The crystal of LRIG1-LRR belongs to space group $P2_12_12_1$ with one molecule in the asymmetric unit. Data at a resolution of 2.3 Å were used to perform molecular replacement calculations using PHASER [49]. A search model was generated from the coordinates of decorin (PDB entry 1XKU [24]) that were modified by changing all non-identical residues to serine using the online server FFAS03[§]. One top solution was found in the asymmetric unit with the *Z*-scores and log-likelihood gain: RFZ = 4.2,

TFZ = 9.4, and LLG = 127. The resulting model had reasonable packing although it did not refine to an acceptable *R*-factor. Subsequently PHENIX [50] automated building and morphing routines were used to produce a model that comprised 274 residues from 454 residues. Further rounds of refinement and manual rebuilding were undertaken using PHENIX [50] and Coot [51]. Statistics for the final model are listed in Table 1.

The crystal of LRIG1-3Ig belongs to space group $P4_32_12$. A search model was produced in the same way as the LRIG1-LRR model by using FFAS03 from the structure of the Titin I1 domain (PDB code 1G1C [52]). PHASER found two of the three Ig domains. This initial model was refined with PHENIX [50] and manual rebuilding was undertaken using Coot [51]. These two domains corresponded to the second and third Ig domains of LRIG1-3Ig. The first Ig domain was manually built into the model by using the coordinates of LRIG3-Ig1 structure (PDB code 3SO5).

Immunofluorescence staining

SW480 and SW620 cells (5×10^3/well) were preincubated in Ibidi chamber slides (Ibidi, Germany) for 3 days then stimulated with or without EGF (100 ng/mL) at 37 °C for 15 min. After washing with PBS (*p*hosphate-*b*uffered *s*aline), we incubated the cells with or without FLAG-LRIG1-LRR-1Ig (1 μM) at 4 °C for 45 min. The cells were washed with PBS and stained with the mouse anti-EGFR antibody 528 [53] or with the mouse anti-FLAG antibody (Sigma-Aldrich; cat. no. A2220) to detect the FLAG-LRIG1-LRR followed by staining with Alexa 488-labelled anti-mouse Ig (Invitrogen; cat. no. A11001). Both bright field and fluorescence images were captured.

Cell culture, reagents, and antibodies

The human embryonic kidney cell line 293T HEK293T and the human epidermoid carcinoma cell line A431 that expresses high levels of the epidermal growth factor (EGF) receptor were maintained in Dulbecco's modified Eagle's medium (DMEM) containing 10% bovine calf serum (BCS) (HyClone) at 37 °C in a 10% CO_2 incubator. Full-length human LRIG1 cDNA construct was purchased from OriGene (cat. no. RC223584), which contains a C-terminal Myc-DDK tag that allows detection by both the anti-Myc and the anti-FLAG antibodies. X-tremeGENE HP DNA transfection reagent and complete protease inhibitor EDTA-free mixture tablets were obtained from Roche Diagnostics. Anti-FLAG-M2-agarose resin was from Sigma-Aldrich. Bovine serum albumin (BSA) fraction V and NuPAGE precast gels were from Life Technologies. PVDF-Plus membrane was from GE Water & Process Technologies. Protein G-Sepharose resin, Amersham ECL kit, ECL film, and donkey anti-rabbit-Ig-HRP and sheep anti-mouse-Ig-HRP were from GE Healthcare. ECL Luminata Forte reagent and mouse anti-phosphotyrosine mAb (*m*onoclonal *anti*body), clone 4G10 (cat. no. 05-321), were from Millipore. Mouse anti-EGFR mAb 806 was produced at the Antibody Production Facility of the Ludwig Institute for Cancer Research, Heidelberg. Rabbit anti-Erk1/2 antibody (cat. no. 9101) was from Cell Signaling Technology. Rat anti-FLAG mAb (clone 9H1) and mouse anti-Myc mAb (clone 9E10) were from the WEHI Antibody Facility.

EGFR phosphorylation inhibition assay

Two days before the assay, A431 cells were seeded in two 6-well plates at 0.5×10^6 cells/well (plate 1) and 0.15×10^6 cells/well (plate 2), respectively. When cells reached confluence, culture medium in plate 1 was removed and 1.5 mL of either recombinant LRIG1-LRR or LRIG1-3Ig was added to wells at 0, 10, and 100 μg/mL, respectively, in DMEM/10% (vol/vol) BCS. For plate 2, culture medium was removed and cells in each well were rinsed once with 3 mL of DMEM containing 0.1% BSA once and then 1.5 mL of either recombinant LRIG1-LRR or LRIG1-3Ig was added to wells also at 0, 10, and 100 μg/mL, respectively. Cells were incubated at 37 °C for a further 2 h in DMEM/0.2% BSA fraction V. The medium was removed and cells were washed once with 3 mL of ice-cold mouse-tonicity PBS and lysed in plates with 150 μL of lysis buffer containing 1% (vol/vol) Triton X-100, 50 mM Tris–HCl (pH 7.5), 150 mM NaCl, and 1 mM EDTA, freshly supplemented with 2 mM Na_3VO_4, 10 mM NaF, 1 mM PMSF, and complete protease inhibitor mixture. Protein extracts were separated by SDS-PAGE, followed by Western blot analysis.

Transient transfection and expression of full-length FLAG-Myc-tagged LRIG1 in A431 cells

One day before transfection, A431 cells were seeded in T150 flasks at 8×10^6 cells/flask in 40 mL of DMEM/10% BCS. Cells in parallel flasks were transfected with 10 μg of full-length FLAG-tagged LRIG1 cDNA construct from OriGene or an empty vector using X-tremeGENE HP DNA transfection reagent according to the manufacturer's instructions. At 48 h posttransfection, medium was removed and cells were rinsed twice with 50 mL of ice-cold normal saline and lysed on ice for 1 h in NP-40 lysis buffer containing 1% (vol/vol) NP-40, 10% (vol/vol) glycerol, 2 mM Na_3VO_4, 10 mM NaF, 1 mM PMSF, and complete protease inhibitor EDTA-free mixture in 50 mM Tris–HCl (pH 7.4) and 150 mM NaCl. Whole cell lysates were cleared by centrifugation at 16,000*g* for 15 min at 4 °C, followed by immunoprecipitation with 50 μL of anti-FLAG M2-agarose beads for 2 h at 4 °C on a rotating wheel. The M2 beads were washed, washed first with 10 mL cold normal saline then three times with 5 mL of NP-40 lysis buffer. Bound proteins were first eluted at 4 °C for 10 min with 400 μL of 1 mg/mL FLAG peptide, followed by a second elution with 400 μL of 0.5% SDS. Eluted proteins and residual beads were separated by SDS-PAGE, followed by Western blot analysis.

Transient transfection of full-length FLAG-Myc-tagged LRIG1 and FLAG-tagged EGFR in HEK293 cells

To examine the interaction between LRIG1 and EGFR, we transfected HEK293T cells with full-length LRIG1 cDNA construct from OriGene, full-length EGFR cDNA construct, or a combination of these two constructs.

Transfection and cell lysis were performed identically as described for A431 cells. Co-immunoprecipitation was performed using 6 μg of anti-Myc mAb 9E10 and 20 μL of protein G-Sepharose beads for 2 h at 4 °C on a wheel. The protein G beads were washed three times each with 1 mL of lysis buffer and bound proteins (immunoprecipitates) eluted from the beads with Laemmli-reducing SDS sample buffer. Immunoprecipitates were separated by SDS-PAGE, followed by Western blot analysis.

Analysis of LRIG1-LRR interaction with $EGFR_{1–621}$ and $EGFR_{1–501}$-Fc [54] by gel-filtration chromatography

We mixed 190 μg of $EGFR_{1–501}$-Fc [36] with 120 μg of LRIG1-LRR in a volume of 500 μL and concentrated them to 50 μL using Amicon centrifugal filter unit (Merck Millipore). The protein mixture was incubated on ice for 2 h and loaded onto a pre-packed Superdex 200 column (300 × 10 mm from GE Healthcare) equilibrated in 25 mM Hepes (pH 7.4) containing 100 mM NaCl and chromatographed at a flow rate of 0.5 mL/min. Aliquots (20 μL) of column fractions (0.5 mL) were analysed by SDS-PAGE and Coomassie blue staining.

Biosensor analysis: Interaction analysis using surface plasmon resonance

Protein–protein interaction was analysed using a Biacore 3000 biosensor. EGFR proteins were immobilised to a CM5 chip by amine coupling according to the manufacturer's instructions to between 2000 and 4000 RU. LRIG1-LRR-1Ig and LRIG1-3Ig fragments and EGF were diluted in 10 mM Hepes, 150 mM NaCl, 3 mM EDTA, and 0.005% Tween 20 (pH 7.4) and were injected over the flow cells at 10 μL/min for 12 min, followed by dissociation for 23 min. The surfaces were regenerated with 50 μL of 10 mM glycine–HCl (pH 2.5) at 50 μL/min. Bulk effects were subtracted using a blank flow cell and rate constants were calculated using BIAevaluation software.

Accession numbers

Accession numbers are as follows: 4U7L for LRR and 4U7M for 3Ig.

Supplementary data to this article can be found online at http://dx.doi.org/10.1016/j.jmb.2015.03.001.

Acknowledgements

We thank P. M. Colman and M. Lawrence for structural insight and continual support. This work was supported in part by funding from the National Health and Medical Research Council under Programme Grants 487922 and 1016647 and Project Grant 1004945. The Ludwig Institute for Cancer Research provided funding for part of this project. This work was made possible through Victorian State Government Operational Infrastructure Support and Australian Government National Health and Medical Research Council Independent Research Institute Infrastructure Support Scheme.

Received 12 September 2014;
Received in revised form 5 February 2015;
Accepted 3 March 2015
Available online 9 March 2015

Keywords:
stem cell marker;
leucine-rich repeat domain;
LINGO-1;
EGFR inhibition

† http://www.uniprot.org/uniprot/O94898.
‡ http://www.uniprot.org/uniprot/Q6UXM1.
§ http://ffas.sanfordburnham.org.

Abbreviations used:
DMEM, Dulbecco's modified Eagle's medium; BSA, bovine serum albumin; BCS, bovine calf serum.

References

[1] Ordonez-Moran P, Huelsken J. Lrig1: a new master regulator of epithelial stem cells. EMBO J 2012;31:2064–6.
[2] Powell AE, Wang Y, Li Y, Poulin EJ, Means AL, Washington MK, et al. The pan-ErbB negative regulator Lrig1 is an intestinal stem cell marker that functions as a tumor suppressor. Cell 2012;149:146–58.
[3] Yan Z, Jiang J, Li F, Yang W, Xie G, Zhou C, et al. Adenovirus-mediated LRIG1 expression enhances the chemosensitivity of bladder cancer cells to cisplatin. Oncol Rep 2015;33:1791–8.
[4] Wong VW, Stange DE, Page ME, Buczacki S, Wabik A, Itami S, et al. Lrig1 controls intestinal stem-cell homeostasis by negative regulation of ErbB signalling. Nat Cell Biol 2012;14:401–8.
[5] Suzuki Y, Sato N, Tohyama M, Wanaka A, Takagi T. cDNA cloning of a novel membrane glycoprotein that is expressed specifically in glial cells in the mouse brain. LIG-1, a protein with leucine-rich repeats and immunoglobulin-like domains. J Biol Chem 1996;271:22522–7.
[6] Laederich MB, Funes-Duran M, Yen L, Ingalla E, Wu X, Carraway KL, et al. The leucine-rich repeat protein LRIG1 is a negative regulator of ErbB family receptor tyrosine kinases. J Biol Chem 2004;279:47050–6.
[7] Gur G, Rubin C, Katz M, Amit I, Citri A, Nilsson J, et al. LRIG1 restricts growth factor signaling by enhancing receptor ubiquitylation and degradation. EMBO J 2004;23:3270–81.
[8] Stutz MA, Shattuck DL, Laederich MB, Carraway KL, Sweeney C. LRIG1 negatively regulates the oncogenic EGF receptor mutant EGFRvIII. Oncogene 2008;27:5741–52.
[9] Goldoni S, Iozzo R, Kay P, Campbell S, McQuillan A, Agnew C, et al. A soluble ectodomain of LRIG1 inhibits cancer cell growth by attenuating basal and ligand-dependent EGFR activity. Oncogene 2007;26:368–81.

[10] Johansson M, Oudin A, Tiemann K, Bernard A, Golebiewska A, Keunen O, et al. The soluble form of the tumor suppressor Lrig1 potently inhibits *in vivo* glioma growth irrespective of EGF receptor status. Neuro Oncol 2013;15:1200–11.
[11] Ledda F, Bieraugel O, Fard SS, Vilar M, Paratcha G. Lrig1 is an endogenous inhibitor of Ret receptor tyrosine kinase activation, downstream signaling, and biological responses to GDNF. J Neurosci 2008;28:39–49.
[12] Lu L, Teixeira VH, Yuan Z, Graham TA, Endesfelder D, Kolluri K, et al. LRIG1 regulates cadherin-dependent contact inhibition directing epithelial homeostasis and pre-invasive squamous cell carcinoma development. J Pathol 2013;229: 608–20.
[13] Nakamura T, Hamuro J, Takaishi M, Simmons S, Maruyama K, Zaffalon A, et al. LRIG1 inhibits STAT3-dependent inflammation to maintain corneal homeostasis. J Clin Invest 2014;124: 385–97.
[14] Lee JM, Kim B, Lee SB, Jeong Y, Oh YM, Song YJ, et al. Cbl-independent degradation of Met: ways to avoid agonism of bivalent Met-targeting antibody. Oncogene 2014;33: 34–43.
[15] Shattuck DL, Miller JK, Laederich M, Funes M, Petersen H, Carraway KL, et al. LRIG1 is a novel negative regulator of the Met receptor and opposes Met and Her2 synergy. Mol Cell Biol 2007;27:1934–46.
[16] Simion C, Cedano-Prieto ME, Sweeney C. The LRIG family: enigmatic regulators of growth factor receptor signaling. Endocr Relat Cancer 2014;21:R431–43.
[17] Rafidi H. Lrig1 negative regulatory activity towards ErbB receptors is opposed by Lrig3. Davis: University of California; 2014.
[18] Nilsson J, Vallbo C, Guo D, Golovleva I, Hallberg B, Henriksson R, et al. Cloning, characterization, and expression of human LIG1. Biochem Biophys Res Commun 2001; 284:1155–61.
[19] Mosyak L, Wood A, Dwyer B, Buddha M, Johnson M, Aulabaugh A, et al. The structure of the Lingo-1 ectodomain, a module implicated in central nervous system repair inhibition. J Biol Chem 2006;281:36378–90.
[20] Coffey RJ, Shipley GD, Moses HL. Production of transforming growth factors by human colon cancer lines. Cancer Res 1986;46:1164–9.
[21] Jensen KB, Collins CA, Nascimento E, Tan DW, Frye M, Itami S, et al. Lrig1 expression defines a distinct multipotent stem cell population in mammalian epidermis. Cell Stem Cell 2009;4:427–39.
[22] Wang Y, Poulin EJ, Coffey RJ. LRIG1 is a triple threat: ERBB negative regulator, intestinal stem cell marker and tumour suppressor. Br J Cancer 2013;108:1765–70.
[23] Heyworth CM, Hampson J, Dexter TM, Walker F, Burgess AW, Kan O, et al. Development of multipotential haemopoietic stem cells to neutrophils is associated with increased expression of receptors for granulocyte macrophage colony-stimulating factor: altered biological responses to GM-CSF during development. Growth Factors 1991;5:87–98.
[24] Scott PG, McEwan PA, Dodd CM, Bergmann EM, Bishop PN, Bella J. Crystal structure of the dimeric protein core of decorin, the archetypal small leucine-rich repeat proteoglycan. Proc Natl Acad Sci U S A 2004;101:15633–8.
[25] Kobe B, Kajava AV. The leucine-rich repeat as a protein recognition motif. Curr Opin Struct Biol 2001;11:725–32.
[26] Kim HM, Oh SC, Lim KJ, Kasamatsu J, Heo JY, Park BS, et al. Structural diversity of the hagfish variable lymphocyte receptors. J Biol Chem 2007;282:6726–32.
[27] Morlot C, Thielens NM, Ravelli RB, Hemrika W, Romijn RA, Gros P, et al. Structural insights into the Slit-Robo complex. Proc Natl Acad Sci 2007;104:14923–8.
[28] He XL, Bazan JF, McDermott G, Park JB, Wang K, Tessier-Lavigne M, et al. Structure of the Nogo receptor ectodomain: a recognition module implicated in myelin inhibition. Neuron 2003;38:177–85.
[29] Seiradake E, Coles CH, Perestenko PV, Harlos K, McIlhinney RAJ, Aricescu AR, et al. Structural basis for cell surface patterning through NetrinG–NGL interactions. EMBO J 2011;30:4479–88.
[30] Williams AF. A year in the life of the immunoglobulin superfamily. Immunol Today 1987;8:298–303.
[31] Lawrence MC, Colman PM. Shape complementarity at protein/protein interfaces. J Mol Biol 1993;234:946–50.
[32] Sasaki T, Knyazev PG, Clout NJ, Cheburkin Y, Göhring W, Ullrich A, et al. Structural basis for Gas6–Axl signalling. EMBO J 2006;25:80–7.
[33] King IC, Catino JJ. Nonradioactive ligand binding assay for epidermal growth factor receptor. Anal Biochem 1990;188: 97–100.
[34] Johns TG, Adams TE, Cochran JR, Hall NE, Hoyne PA, Olsen MJ, et al. Identification of the epitope for the epidermal growth factor receptor-specific monoclonal antibody 806 reveals that it preferentially recognizes an untethered form of the receptor. J Biol Chem 2004;279:30375–84.
[35] Goetz M, Ziebart A, Foersch S, Vieth M, Waldner MJ, Delaney P, et al. *In vivo* molecular imaging of colorectal cancer with confocal endomicroscopy by targeting epidermal growth factor receptor. Gastroenterology 2010;138:435–46.
[36] Elleman TC, Domagala T, McKern NM, Nerrie M, Lönnqvist B, Adams TE, et al. Identification of a determinant of epidermal growth factor receptor ligand-binding specificity using a truncated, high-affinity form of the ectodomain. Biochemistry 2001;40:8930–9.
[37] Bai L, McEachern D, Yang CY, Lu J, Sun H, Wang S. LRIG1 modulates cancer cell sensitivity to Smac mimetics by regulating TNFalpha expression and receptor tyrosine kinase signaling. Cancer Res 2012;72:1229–38.
[38] Chang L, Shi R, Yang T, Li F, Li G, Guo Y, et al. Restoration of LRIG1 suppresses bladder cancer cell growth by directly targeting EGFR activity. J Exp Clin Cancer Res 2013;32: 101.
[39] Hamburger AW. The role of ErbB3 and its binding partners in breast cancer progression and resistance to hormone and tyrosine kinase directed therapies. J Mammary Gland Biol Neoplasia 2008;13:225–33.
[40] Ljuslinder I, Golovleva I, Palmqvist R, Oberg A, Stenling R, Jonsson Y, et al. LRIG1 expression in colorectal cancer. Acta Oncol 2007;46:1118–22.
[41] Suzuki Y, Miura H, Tanemura A, Kobayashi K, Kondoh G, Sano S, et al. Targeted disruption of LIG-1 gene results in psoriasiform epidermal hyperplasia. FEBS Lett 2002;521:67–71.
[42] Gaj T, Gersbach CA, Barbas CF. ZFN, TALEN, and CRISPR/Cas-based methods for genome engineering. Trends Biotechnol 2013;31:397–405.
[43] Xu Y, Kershaw NJ, Luo CS, Soo P, Pocock MJ, Czabotar PE, et al. Crystal structure of the entire ectodomain of gp130: insights into the molecular assembly of the tall cytokine receptor complexes. J Biol Chem 2010;285:21214–8.
[44] Carrington JC, Dougherty WG. A viral cleavage site cassette: identification of amino acid sequences required for tobacco etch virus polyprotein processing. Proc Natl Acad Sci 1988; 85:3391–5.

[45] Hopp TP, Prickett KS, Price VL, Libby RT, March CJ, Cerretti DP, et al. A short polypeptide marker sequence useful for recombinant protein identification and purification. Biotechnology 1988;6:1204–10.
[46] Walker F, deBlaquiere J, Burgess AW. Translocation of pp60c-src from the plasma membrane to the cytosol after stimulation by platelet-derived growth factor. J Biol Chem 1993;268:19552–8.
[47] Kabsch W. Integration, scaling, space-group assignment and post-refinement. Acta Crystallogr D Biol Crystallogr 2010;66:133–44.
[48] Karplus PA, Diederichs K. Linking crystallographic model and data quality. Science 2012;336:1030–3.
[49] McCoy AJ, Grosse-Kunstleve RW, Adams PD, Winn MD, Storoni LC, Read RJ. Phaser crystallographic software. J Appl Crystallogr 2007;40:658–74.
[50] Adams PD, Afonine PV, Bunkóczi G, Chen VB, Davis IW, Echols N, et al. PHENIX: a comprehensive Python-based system for macromolecular structure solution. Acta Crystallogr D Biol Crystallogr 2010;66:213–21.
[51] Emsley P, Lohkamp B, Scott W, Cowtan K. Features and development of Coot. Acta Crystallogr D Biol Crystallogr 2010;66:486–501.
[52] Mayans O, Wuerges J, Canela S, Gautel M, Wilmanns M. Structural evidence for a possible role of reversible disulphide bridge formation in the elasticity of the muscle protein titin. Structure 2001;9:331–40.
[53] Sato J, Kawamoto T, Le A, Mendelsohn J, Polikoff J, Sato G. Biological effects *in vitro* of monoclonal antibodies to human epidermal growth factor receptors. Mol Biol Med 1983;1:511–29.
[54] Adams TE, Koziolek EJ, Hoyne PH, Bentley JD, Lu L, Lovrecz G, et al. A truncated soluble epidermal growth factor receptor-Fc fusion ligand trap displays anti-tumour activity *in vivo*. Growth Factors 2009;27:141–54.
[55] Tan CW, Hirokawa Y, Gardiner BS, Smith DW, Burgess AW. Colon cryptogenesis: asymmetric budding. PLoS One 2013;8:e78519.